




RESEARCH ARTICLE | JANUARY 31 2024


Surface wave interaction with floating elastic plates in channels

K. Ren (任康) ; G. X. Wu (吴国雄)  ; Y. F. Yang (杨毅锋) 




Physics of Fluids 36, 017143 (2024)

<https://doi.org/10.1063/5.0185714>



Physics of Fluids
Special Topic:
Flow and Climate
Guest Editors: Khaled Ghannam and Mostafa Momen
[Submit Today!](#)



Surface wave interaction with floating elastic plates in channels

Cite as: Phys. Fluids **36**, 017143 (2024); doi: [10.1063/5.0185714](https://doi.org/10.1063/5.0185714)

Submitted: 1 November 2023 · Accepted: 7 January 2024 ·

Published Online: 31 January 2024



View Online



Export Citation



CrossMark

K. Ren (任康), G. X. Wu (吴国雄), ^{a)} and Y. F. Yang (杨毅锋)

AFFILIATIONS

Department of Mechanical Engineering, University College London, Torrington Place, London WC1E 7JE, United Kingdom

^{a)} Author to whom correspondence should be addressed: g.wu@ucl.ac.uk

ABSTRACT

The interaction between surface waves and a finite rectangular floating plate in a channel is considered analytically, while the location of the plate is not restricted. The mathematical model is based on the linear velocity potential flow theory for the fluid and the Kirchhoff–Love plate theory for the plate. The problem is converted into an integral equation through using the Green function. The second-order singularity associated with a body with no thickness is treated with the Dirac delta function. The developed scheme is used for case studies of various edge constraints. Extensive results are provided for the hydrodynamic forces acting on the plate and the wave reflection and transmission coefficients. The effects of wave frequency, channel width, plate length, and edge conditions are analyzed, and their physical implications are highlighted. Significant findings comprise the highly oscillatory nature of force curves, influenced by the natural frequencies of the channels and the length of the plate, and substantial effects of edge conditions and the plate position on the results.

© 2024 Author(s). All article content, except where otherwise noted, is licensed under a Creative Commons Attribution (CC BY) license (<http://creativecommons.org/licenses/by/4.0/>). <https://doi.org/10.1063/5.0185714>

I. INTRODUCTION

The propagation of water waves and their interaction with structures in channels or long tanks play a crucial role in hydrodynamics. These issues have wide-ranging implications, such as in ship navigation safety, carbon emissions and associated costs, breakwater design, and the generation of renewable energy. In addition, in the field of marine engineering, model tests are commonly conducted in towing and wave tanks, and the effects of tank walls are quite often not insignificant. Unlike problems of a prototype in open water, the presence of transverse mode flow across the tank and its resonant motion may significantly affect the hydrodynamic performance of a model in the tank, particularly when the motion frequency is near one of the natural frequencies of the tank. It is, therefore, important to understand the nature of the side wall effect when the measured results for the model are converted to those for the prototype in the open sea.

Extensive research has been carried out on free surface wave interaction with structures in a channel. Eatock Taylor and Hung¹ and Yeung and Sphaier² adopted the method of images to study wave radiation and diffraction by a vertical cylinder along the centerline of a channel. Linton and Evans³ investigated a similar problem by constructing channel multipoles, while McIver and Bennett⁴ considered off-center scenarios. Wave diffraction by an array of vertical cylinders in a channel was further investigated by Linton and McIver.⁵ Trapped

modes may occur for surface wave interaction with rigid bodies in a channel, as demonstrated in Refs. 6–11. For submerged spheres, Wu^{12,13} and Ursell^{14–16} carried out a series of studies on its interaction with surface waves in a channel using multipole expansion approaches. In addition, the interaction between an oscillating wave energy converter (OWEC) and water waves in a channel was studied by Renzi and Dias,¹⁷ and the motion responses of the device near the natural frequencies of the channel were investigated through parametric studies.

The above-mentioned works are all about the interaction of surface waves with rigid bodies. When an elastic cover is placed on the water surface in a channel, the motion of the surface waves and the vibration of the elastic cover are coupled. The propagation of flexural gravity or hydro-elastic waves in a channel is very different from surface waves, as discussed by Korobkin *et al.*¹⁸ and Ren *et al.*¹⁹ An efficient analytical scheme has been developed by Ren *et al.*¹⁹ to investigate the traveling modes of hydro-elastic waves corresponding to various edge conditions along the channel walls and has been extended to study the effect of a longitudinal line crack on the cover. Based on the expansions in Ren *et al.*,¹⁹ the Green function satisfying all boundary conditions apart from the body surface has been derived. Solution procedures were further developed for the interaction between a uniform current and a horizontal cylinder below the elastic

plate cover²⁰ and the interaction of the hydro-elastic waves with a vertical cylinder.²¹ In addition, experimental research on the interaction of surface waves with floating and submerged finite rectangular plates can be found in the works of Dolatshah *et al.*²² and Want *et al.*²³

The objective of this study is to investigate the interaction between surface waves and non-rigid bodies in restricted waters, such as channels. Our focus is on a finite elastic floating plate. We have developed an analytical solution scheme based on the Green function technique. The method provides flexibility for different edge constraints and gives insight into the nature of the hydrodynamic forces as well as flow features within the channel. In addition, the energy identity is also re-derived for an elastic body. It is also worth mentioning that Porter²⁴ considered a similar problem of a rectangular floating ice sheet in an unbounded ocean, focusing solely on the free edge constraint. The deflection of the plate was expanded based on the free vibration modes with the unknown coefficients. Each free vibration mode is further expanded based on the product of two eigenmode series, corresponding to the expansion of one-dimensional Euler–Bernoulli beam functions in each direction. The eigenvalue and eigenvector of the free vibration mode are obtained through a variation statement that enforces satisfaction of the free vibration equation and the free edge condition. The unknown coefficients are obtained through the integral equation with the Rayleigh–Ritz method. In the present work, we also employ a boundary integral equation technique. However, in addition to the side wall effect of the channel, we adopt a different procedure for the deflection. Using the dynamic equation of the elastic plate, the integral equation will become one with dipole distribution over the plate, whose strength can be written in terms of the deflection of the plate and its spatial derivatives. Through the kinematic condition of fluid flow on the plate surface, a governing equation for the plate deflection can be obtained. In contrast to Porter,²⁴ we expand the plate deflection into a double cosine series, together with four additional terms of simple polynomial functions in each direction for edge conditions. The rationale behind this has been explained by Ren *et al.*^{19,25} In addition to the fact that this kind of shape function is much simpler, this avoids the step of solving the free vibration modes. The deflection can be obtained directly from the solution of the integral equation. This approach also offers much more flexibility. For different edge conditions, the coefficients of the four additional terms in the expansion can be adjusted to meet these conditions. This method can, therefore, be easily used for any given edge conditions. It is worth mentioning that special attention should be given to the term of second-order singularity in the integral, as discussed by Martin and Farina²⁶ for a thin rigid disc submerged under a free surface undergoing heave motion. In the present work, since we adopt a double series form for the Green function of the free surface channel, the effect of the singularity can be reflected through the non-convergence of the series. To treat that, we adopt a direct approach, through using the Dirac delta function. The developed boundary integral scheme allows us to consider a horizontal thin plate with an arbitrary finite length, width, and position within the channel. Specifically, to verify the solution procedure, an alternative scheme based on series expansion has been developed for the case of a floating plate of the same width as the channel.

The outlines of this paper are as follows: the mathematical modeling and solution procedure are introduced in Sec. II. Extensive results and analysis are then provided in Sec. III for wave loads, reflection and

transmission coefficients, and the deflection of the plate in scenarios involving a floating plate on or off the centerline. Finally, conclusions are drawn in Sec. IV.

II. MATHEMATICAL MODELING AND SOLUTION PROCEDURE

We consider the interaction between water waves and a floating horizontal rectangular plate in a wave tank, which is treated as an infinitely long channel of finite depth. The sketch of the problem is displayed in Fig. 1. A Cartesian coordinate system $O-xyz$ is established with the origin located on the centerline of the undisturbed free surface. The x - and y -axes are along the longitudinal and transverse directions of the channel, respectively, while its z -axis is pointing upward. Two sides of the plate are parallel to the walls of the channel, while any other orientation can be easily treated through a coordinate transformation. The coordinates of the center of the plate are $(x_c, y_c, 0)$, where x_c can be set as zero without loss of generality. The half-width of the channel is denoted as b , while the half-length and half-width of the plate are denoted as l and b_p , respectively.

A. Governing equations and boundary conditions

The velocity potential theory and the Kirchhoff–Love plate theory are used for the fluid flow and the elastic plate vibration, respectively. For the former, it assumes that the fluid is incompressible and inviscid, and its motion is irrotational. When the incoming wave of amplitude A_0 is sinusoidal in time with frequency ω , the velocity potential and the deflection of the plate may be, respectively, written as $\Phi(x, y, z, t) = \text{Re}\{A_0\phi(x, y, z) e^{i\omega t}\}$ and $W(x, y, t) = \text{Re}\{A_0 w(x, y) e^{i\omega t}\}$. The problem can then be solved in the frequency domain.

The complex velocity potential $\phi(x, y, z)$ satisfies the Laplace equation throughout the fluid domain, or

$$\frac{\partial^2 \phi}{\partial x^2} + \frac{\partial^2 \phi}{\partial y^2} + \frac{\partial^2 \phi}{\partial z^2} = 0. \tag{1}$$

The complex deflection $w(x, y)$ of the horizontal elastic plate at $z = 0$ is governed by the following equation:

$$L\nabla^4 w - \omega^2 \rho_c h w = p, \tag{2}$$

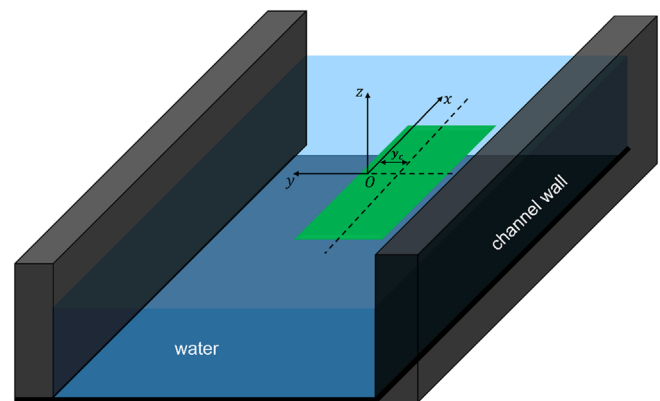


FIG. 1. The sketch of the problem.

where $L = Eh^3/[12(1 - \nu^2)]$ is the flexural rigidity, with h , ρ_e , and ν being the thickness, density, and Poisson's ratio of the plate, respectively. $\rho_e h$ refers to the mass per unit area of the plate. p is the difference between the hydrodynamic pressure on the lower side of the plate and atmospheric pressure, which can be written as

$$p = -\rho g w - i\rho\omega\phi|_{z=0}. \tag{3}$$

At the interface of fluid and the plate, the linearized kinematic condition can be given as

$$i\omega w = \frac{\partial\phi}{\partial z}\Big|_{z=0} \quad (|x| \leq l, |y - y_c| \leq b_p). \tag{4}$$

In addition, the linearized free surface boundary condition can be given as

$$\phi_z - \gamma\phi = 0, \quad (|x| > l, \text{ or } |y - y_c| > b_p, z = 0), \tag{5}$$

where $\gamma = \omega^2/g$ and g is the acceleration due to gravity. The bottom and channel walls are assumed to be rigid, and the impermeable boundary condition gives

$$\frac{\partial\phi}{\partial y}\Big|_{y=\pm b} = \frac{\partial\phi}{\partial z}\Big|_{z=-H} = 0. \tag{6}$$

In the far field at $x = \pm\infty$, the radiation condition ensures that every component of the diffracted potential, denoted as ψ , corresponds to an outgoing wave. We have

$$\lim_{x \rightarrow \pm\infty} \left(\frac{\partial}{\partial x} \mp iK \right) \psi \rightarrow 0,$$

where K refers to the wave number of the outgoing wave.

In addition, edge conditions are essential for plate problems. Three common conditions for a curved edge shape can be written as²⁷

$$w = 0, \quad w_n = 0, \tag{7}$$

for the clamped edge,

$$\nabla^2 w = (1 - \nu) \left[\frac{\partial^2}{\partial s^2} + \frac{1}{\mathcal{R}} \frac{\partial}{\partial n} \right] w, \tag{8}$$

$$\frac{\partial}{\partial n} [\nabla^2 w] = -(1 - \nu) \frac{\partial}{\partial s} \left[\frac{\partial^2}{\partial s \partial n} - \frac{1}{\mathcal{R}} \frac{\partial}{\partial s} \right] w$$

for the free edge, and

$$w = 0, \quad \nabla^2 w = (1 - \nu) \left[\frac{\partial^2}{\partial s^2} + \frac{1}{\mathcal{R}} \frac{\partial}{\partial n} \right] w, \tag{9}$$

for the simply supported edge. Derivatives with respect to n and s refer to variations along the normal and tangential directions of the edge, respectively. \mathcal{R} is the radius of curvature.

B. Boundary integral method

The boundary integral method is adopted to solve the boundary value problem mentioned above. The Green function for a free-surface channel satisfying $\nabla^2 G = 2\pi\delta(x - x_0)\delta(y - y_0)\delta(z - z_0)$ can be written as²⁸

$$G(x, y, z; x_0, y_0, z_0) = \sum_{m=0}^{\infty} \sum_{n=0}^{\infty} \frac{i\pi \cosh k_m(z_0 + H) \cos \beta_n(y_0 + b) \cosh k_m(z + H) \cos \beta_n(y + b)}{\tau_{mn}(1 + \delta_{n0})b \left(\frac{2k_m H + \sinh 2k_m H}{4k_m} \right)} e^{-i\tau_{mn}|x-x_0|}. \tag{10}$$

where $\beta_n = n\pi/2b$, $\tau_{mn}^2 = k_m^2 - \beta_n^2$, and k_m are solutions of the dispersion relation obtained by substituting (10) into (5) or

$$k \tanh kH = \gamma. \tag{11}$$

It should be noted that the roots of (11) include a positive real one k_0 and an infinite number of positive imaginary ones k_m , $m = 1, 2, \dots$. For $k_0^2 > \beta_n^2$, τ_{0n} is a real number that should be taken as positive to ensure that the wave is outgoing. In addition, to ensure that (10) is finite, when τ_{mn} is complex, its imaginary part should be taken as negative.

When the Green's second identity is applied to the diffraction velocity potential, or ϕ_D , and the Green function G , we have

$$\phi_D(x_0, y_0, z_0) = \frac{1}{2\pi} \oint_S \left(\phi_D \frac{\partial G}{\partial n} - G \frac{\partial \phi_D}{\partial n} \right) dS, \tag{12}$$

where S is the surface of the entire fluid domain, containing the bottom S_B and side walls S_W of the channel, the free surface S_F , the two far-field boundaries $S_{\pm\infty}$ at $x = \pm\infty$, respectively, and S_p is the lower surface of the plate. By applying boundary conditions on S_B , S_W , S_F , and $S_{\pm\infty}$, (12) can be reduced to

$$\phi_D(x_0, y_0, z_0) = \frac{1}{2\pi} \iint_{S_p} \left(\phi_D \frac{\partial G}{\partial n} - G \frac{\partial \phi_D}{\partial n} \right) dS. \tag{13}$$

Noting that $\phi_D = \phi - \phi_I$ where ϕ is the total potential, we have

$$\begin{aligned} \phi(x_0, y_0, z_0) - \phi_I &= \frac{1}{2\pi} \iint_{S_p} \left(\phi \frac{\partial G}{\partial n} - G \frac{\partial \phi}{\partial n} \right) dS \\ &+ \frac{1}{2\pi} \iint_{S_p} \left(G \frac{\partial \phi_I}{\partial n} - \phi_I \frac{\partial G}{\partial n} \right) dS. \end{aligned} \tag{14}$$

The second integration on the right-hand side of (14) is zero if the free surface boundary conditions of G and ϕ_I on $z = 0$ are used. Equation (14) can then be written as

$$\phi(x_0, y_0, z_0) - \phi_I = \frac{1}{2\pi} \iint_{S_p} \left(\phi \frac{\partial G}{\partial n} - G \frac{\partial \phi}{\partial n} \right) dS. \tag{15}$$

Substituting (2) and (4) into (15), we have

$$\phi(x_0, y_0, z_0) - \phi_I = \frac{i}{2\pi\rho\omega} \iint_{S_p} (L\nabla^4 w - \omega^2\rho_e h w) \frac{\partial G}{\partial z} dS. \tag{16}$$

Differentiating (16) with respect to z_0 at $z_0 \rightarrow 0$ and further using (4), we have

$$i\omega w - \frac{\partial \phi_I}{\partial z_0} \Big|_{z_0 \rightarrow 0} = \frac{i}{2\pi\rho\omega} \iint_{S_p} (L\nabla^4 w - \omega^2 \rho_e h w) \left[\frac{\partial G}{\partial z \partial z_0} \right]_{z_0 \rightarrow 0, z=0} dS, \tag{17}$$

where (x_0, y_0) are on S_p . The deflection w can be further expanded as²⁵

$$w = \sum_{n=0}^{\infty} \sum_{j=0}^{\infty} C_{nj} \times \cos \alpha_j(x+l) \cos \tilde{\beta}_n(y_1 + b_p) + \sum_{n=0}^{\infty} \cos \tilde{\beta}_n(y_1 + b_p) \cdot f_n(x) + \sum_{j=0}^{\infty} \cos \alpha_j(x+l) \cdot g_j(y_1), \tag{18}$$

where $y_1 = y - y_c$ with $y_1 = 0$ being the longitudinal centerline of the plate, $\alpha_j = j\pi/2l$, $\tilde{\beta}_n = n\pi/2b_p$ and

$$f_n(x) = d_n^{(1)} \left(\frac{x}{l}\right) + d_n^{(2)} \left(\frac{x}{l}\right)^2 + d_n^{(3)} \left(\frac{x}{l}\right)^3 + d_n^{(4)} \left(\frac{x}{l}\right)^4, \tag{19}$$

$$g_j(y_1) = c_j^{(1)} \left(\frac{y_1}{b_p}\right) + c_j^{(2)} \left(\frac{y_1}{b_p}\right)^2 + c_j^{(3)} \left(\frac{y_1}{b_p}\right)^3 + c_j^{(4)} \left(\frac{y_1}{b_p}\right)^4. \tag{20}$$

In addition, $\left(\frac{x}{l}\right)^i$ and $\left(\frac{y_1}{b_p}\right)^i$ ($i = 0-4$) can be further expanded as

$$\left(\frac{x}{l}\right)^i = \sum_{j=0}^{\infty} \mu_j^{(i)} \cos \alpha_j(x+l), \tag{21}$$

$$\left(\frac{y_1}{b_p}\right)^i = \sum_{n=0}^{\infty} \mu_n^{(i)} \cos \tilde{\beta}_n(y_1 + b_p). \tag{22}$$

as in Ref. 25, where the expressions for $\mu_j^{(i)}$ can be found. Therefore, from (17), we have

$$\begin{aligned} & \sum_{n=0}^{\infty} \sum_{j=0}^{\infty} \left[C_{nj} + \sum_{i=1}^4 d_n^{(i)} \mu_j^{(i)} + \sum_{i=1}^4 c_j^{(i)} \mu_n^{(i)} \right] \times \psi_{jn}(x_0, y_{01}) \\ &= \frac{1}{i\omega} \frac{\partial \phi_I}{\partial z_0} \Big|_{z_0 \rightarrow 0} + \frac{1}{2\rho\omega^2\pi} \int_{-l}^l \int_{-b_p}^{b_p} (L\nabla^4 w - \omega^2 \rho_e h w) \\ & \times \left[\frac{\partial G}{\partial z \partial z_0} \right]_{z_0 \rightarrow 0, z=0} dy_1 dx, \end{aligned} \tag{23}$$

where $\psi_{jn}(x, y) = \cos \alpha_j(x+l) \cos \tilde{\beta}_n(y + b_p)$, $y_{01} = y_0 - y_c$.

Based on (18), the terms $\nabla^4 w$ and w in the integrand of (23) can be further written as double cosine series as

$$\nabla^4 w = \sum_{n=0}^{\infty} \sum_{j=0}^{\infty} \left[C_{nj} (\alpha_j^2 + \tilde{\beta}_n^2)^2 + \sum_{i=1}^4 \left(\alpha_j^4 \mu_n^{(i)} - \frac{2i(i-1)}{b_p^2} \alpha_j^2 \mu_n^{(i-2)} + \frac{24\delta_{i4} \mu_n^{(0)}}{b_p^4} \right) c_j^{(i)} + \sum_{i=1}^4 \left(\tilde{\beta}_n^4 \mu_j^{(i)} - \frac{2i(i-1)}{l^2} \tilde{\beta}_n^2 \mu_j^{(i-2)} + \frac{24\delta_{i4} \mu_j^{(0)}}{l^4} \right) d_n^{(i)} \right] \psi_{jn}(x, y_1), \tag{24}$$

$$w = \sum_{n=0}^{\infty} \sum_{j=0}^{\infty} \left[C_{nj} + \sum_{i=1}^4 \mu_j^{(i)} d_n^{(i)} + \sum_{i=1}^4 \mu_n^{(i)} c_j^{(i)} \right] \times \psi_{jn}(x, y_1). \tag{25}$$

Here, it is important to note that in (23) derivatives are applied to x^i and y^i first before they are expanded into the cosine series to ensure convergence.¹⁹ Substituting (10), (24), and (25) into (23) and performing the integration with respect to (x, y_1) , we obtain

$$\begin{aligned} & \sum_{n=0}^{\infty} \sum_{j=0}^{\infty} C_{nj} \left\{ \psi_{jn}(x_0, y_{01}) - \left[L(\alpha_j^2 + \tilde{\beta}_n^2)^2 - \omega^2 \rho_e h \right] I_{nj} \right\} \\ & + \sum_{j=0}^{\infty} \sum_{i=1}^4 c_j^{(i)} \sum_{n=0}^{\infty} \left\{ \mu_n^{(i)} \psi_{jn}(x_0, y_{01}) - I_{nj} \left[L \left(\alpha_j^4 \mu_n^{(i)} - \frac{2i(i-1)}{b_p^2} \alpha_j^2 \mu_n^{(i-2)} + \frac{24\delta_{i4} \mu_n^{(0)}}{b_p^4} \right) - \omega^2 \rho_e h \mu_n^{(i)} \right] \right\} \\ & + \sum_{n=0}^{\infty} \sum_{i=1}^4 d_n^{(i)} \sum_{j=0}^{\infty} \left\{ \mu_j^{(i)} \psi_{jn}(x_0, y_{01}) - I_{nj} \left[L \left(\tilde{\beta}_n^4 \mu_j^{(i)} - \frac{2i(i-1)}{l^2} \tilde{\beta}_n^2 \mu_j^{(i-2)} + \frac{24\delta_{i4} \mu_j^{(0)}}{l^4} \right) - \omega^2 \rho_e h \mu_j^{(i)} \right] \right\} = \frac{1}{i\omega} \frac{\partial \phi_I}{\partial z_0} \Big|_{z_0 \rightarrow 0}, \end{aligned} \tag{26}$$

where

$$I_{nj} = \lim_{z_0 \rightarrow 0} \sum_{m=0}^{\infty} \frac{4k_m^3 \sinh k_m H \sinh [k_m(z_0 + H)]}{\rho\omega^2 b(2k_m H + \sinh 2k_m H)} \times \sum_{n'=0}^{\infty} \frac{I_1^{(n,n')}}{(1 + \delta_{n'0})(\alpha_j^2 - \tau_{nn'}^2)} \left[e^{i(\alpha_j - \tau_{nn'})l} \cos(\tau_{nn'} x_0 + \alpha_j l) - \cos \alpha_j(x_0 + l) \right] \cos \beta_{n'}(y_0 + b) \tag{27}$$

and

$$I_1^{(n,n')} = \int_{-b_p}^{b_p} \cos \tilde{\beta}_n(y_1 + b_p) \cos \beta_{n'}(y + b) dy_1 = \frac{\beta_{n'} [\sin [\beta_{n'}(b + b_p + y_c) - 2\tilde{\beta}_n b_p] - \sin \beta_{n'}(b - b_p + y_c)]}{\beta_{n'}^2 - \tilde{\beta}_n^2}$$

$$= \frac{2\beta_{n'} \sin [(\beta_{n'} - \tilde{\beta}_n)b_p] \cos [\beta_{n'}(b + y_c) - \tilde{\beta}_n b_p]}{\beta_{n'}^2 - \tilde{\beta}_n^2}. \tag{28}$$

When $\tilde{\beta}_n \rightarrow \beta_{n'}$, (28) becomes

$$I_1^{(n,n')} = (1 + \delta_{n0})b_p \cos \tilde{\beta}_n(y_c + b - b_p). \tag{29}$$

Multiplying $\psi_{j^*n^*}(x_0, y_{01})$ on both sides of (26) and integrating with respect to x_0 and y_{01} , respectively, over $[-l, l]$ and $[-b_p, b_p]$, using the orthogonality of cosine functions, we have

$$C_{n^*j^*}(1 + \delta_{j^*0})l(1 + \delta_{n^*0})b_p - \sum_{n=0}^{\infty} \sum_{j=0}^{\infty} C_{nj} \left[L(\alpha_j^2 + \tilde{\beta}_n^2)^2 - \omega^2 \rho_e h \right] \times \mathfrak{I}_{n,j,n^*,j^*} + \sum_{i=1}^4 c_j^{(i)} \mu_n^{(i)} (1 + \delta_{j^*0})l(1 + \delta_{n^*0})b_p$$

$$- \sum_{j=0}^{\infty} \sum_{i=1}^4 c_j^{(i)} \sum_{n=0}^{\infty} \left\{ \left[L \left(\alpha_j^4 \mu_n^{(i)} - \frac{2i(i-1)}{b_p^2} \alpha_j^2 \mu_n^{(i-2)} + \frac{24\delta_{i4} \mu_n^{(0)}}{b_p^4} \right) - \omega^2 \rho_e h \mu_n^{(i)} \right] \times \mathfrak{I}_{n,j,n^*,j^*} \right\}$$

$$+ \sum_{i=1}^4 d_n^{(i)} \mu_{j^*}^{(i)} (1 + \delta_{j^*0})l(1 + \delta_{n^*0})b_p - \sum_{n=0}^{\infty} \sum_{i=1}^4 d_n^{(i)} \sum_{j=0}^{\infty} \left\{ \left[L \left(\tilde{\beta}_n^4 \mu_j^{(i)} - \frac{2i(i-1)}{l^2} \tilde{\beta}_n^2 \mu_j^{(i-2)} + \frac{24\delta_{i4} \mu_j^{(0)}}{l^4} \right) - \omega^2 \rho_e h \mu_j^{(i)} \right] \times \mathfrak{I}_{n,j,n^*,j^*} \right\}$$

$$= \int_{-l}^l \int_{-b_p}^{b_p} \frac{1}{i\omega} \frac{\partial \phi_I}{\partial z_0} \Big|_{z_0=0} \psi_{j^*n^*}(x_0, y_{01}) dx_0 dy_{01} \quad (n^*, j^* = 0, 1, 2, 3, \dots), \tag{30}$$

where

$$\mathfrak{I}_{n,j,n^*,j^*} = -\frac{\delta_{jj^*}(1 + \delta_{j^*0})l}{\rho\omega^2 b} \times \sum_{n^*=0}^{\infty} \frac{I_1^{(n,n')} I_1^{(n^*,n')}}{(1 + \delta_{n^*0})} \lim_{z_0 \rightarrow 0} \sum_{m=0}^{\infty} \frac{4k_m \sinh k_m H \sinh k_m(z_0 + H)}{(2k_m H + \sinh 2k_m H)} \times \frac{k_m^2}{(\alpha_j^2 - \tau_{mn'}^2)}$$

$$+ \lim_{z_0 \rightarrow 0} \sum_{m=0}^{\infty} \frac{2ik_m^3 \sinh k_m H \sinh k_m(z_0 + H)}{\rho\omega^2 b(2k_m H + \sinh 2k_m H)} \times \sum_{n^*=0}^{\infty} \frac{I_1^{(n,n')} I_1^{(n^*,n')} \tau_{mn'} \left\{ 1 + (-1)^{j+j^*} - [(-1)^j + (-1)^{j^*}] e^{-2i\tau_{mn'} l} \right\}}{(1 + \delta_{n^*0})(\alpha_j^2 - \tau_{mn'}^2)(\alpha_{j^*}^2 - \tau_{mn'}^2)}. \tag{31}$$

It is worth noting that

$$-\sum_{m=0}^{\infty} \frac{4k_m \sinh k_m(z + H) \sinh k_m(z_0 + H)}{(2k_m H + \sinh 2k_m H)} = \delta(z - z_0). \tag{32}$$

To obtain (32), we first expand $\delta'(z - z_0)$ into the orthonormal series based on vertical modes $\cosh k_m(z + H)$, which can be obtained as

$$\delta'(z - z_0) = \sum_{m=0}^{\infty} \frac{-4k_m^2 \sinh k_m(z_0 + H) \cosh k_m(z + H)}{2k_m H + \sinh 2k_m H}. \tag{33}$$

We then integrate this with respect to z from $-H$ to z , which gives (32). When $z = 0$ and $z_0 \rightarrow 0$, it follows

$$\lim_{z_0 \rightarrow 0} \sum_{m=0}^{\infty} \frac{-4k_m \sinh k_m(z_0 + H) \sinh k_m H}{(2k_m H + \sinh 2k_m H)} = \lim_{z_0 \rightarrow 0} \delta(0 - z_0) = 0.$$

This can be removed from (31), which gives

$$\begin{aligned} \mathcal{J}_{n,j,n^*,j^*} = & -\frac{\delta_{jj^*}(1 + \delta_{j^*0})l}{\rho\omega^2 b} \times \sum_{n'=0}^{\infty} \frac{I_1^{(n,n')} I_1^{(n^*,n')}}{(1 + \delta_{n'0})} \sum_{m=0}^{\infty} \frac{4k_m \sinh^2 k_m H}{(2k_m H + \sinh 2k_m H)} \times \frac{\beta_{n'}^2 + \alpha_j^2}{(\alpha_j^2 - \tau_{mn'}^2)} + \sum_{m=0}^{\infty} \frac{2ik_m^3 \sinh^2 k_m H}{\rho\omega^2 b(2k_m H + \sinh 2k_m H)} \\ & \times \sum_{n'=0}^{\infty} \frac{I_1^{(n,n')} I_1^{(n^*,n')} \tau_{mn'}}{(1 + \delta_{n'0})(\alpha_j^2 - \tau_{mn'}^2)(\alpha_{j^*}^2 - \tau_{mn'}^2)} \left\{ 1 + (-1)^{j+j^*} - [(-1)^j + (-1)^{j^*}] e^{-2i\tau_{mn'} l} \right\}. \end{aligned} \tag{34}$$

The velocity potential of the incident wave of unit amplitude from $x_0 = -\infty$ can be written as

$$\phi_I(x_0, z_0) = -\frac{g}{i\omega} \times \frac{\cosh k_0(z_0 + H)}{\cosh k_0 H} \times e^{-ik_0 x_0}. \tag{35}$$

Then, the right-hand side of (30) becomes

$$\begin{aligned} & \int_{-l}^l \int_{-b_p}^{b_p} \frac{1}{i\omega} \frac{\partial \phi_I}{\partial z_0} \Big|_{z_0=z_c} \psi_{j^* n^*}(x_0, y_{01}) dx_0 dy_{01} \\ & = \frac{2ik_0 \delta_{n^*0} b_p [-e^{ik_0 l} + e^{-ik_0 l} (-1)^{j^*}]}{k_0^2 - \alpha_{j^*}^2} \\ & = \begin{cases} \frac{-4ik_0 \delta_{n^*0} b_p \cos k_0 l}{k_0^2 - \alpha_{j^*}^2}, & \text{when } j^* \text{ is odd} \\ \frac{4k_0 \delta_{n^*0} b_p \sin k_0 l}{k_0^2 - \alpha_{j^*}^2}, & \text{when } j^* \text{ is even.} \end{cases} \end{aligned} \tag{36}$$

Apart from the equations above, conditions on the plate edge should also be imposed. For the free edge (F-F-F-F), (8) can be written as from $\left[\frac{\partial^2 w}{\partial x^2} + \nu \frac{\partial^2 w}{\partial y_1^2} \right]_{x=\mp l} = 0$:

$$\begin{aligned} & -\sum_{j=0}^{\infty} (\alpha_j^2 + \nu \tilde{\beta}_n^2) (\pm 1)^j C_{nj} + \sum_{i=1}^4 \left(\frac{i(i-1)}{l^2} - \nu \tilde{\beta}_n^2 \right) (\mp 1)^i d_n^{(i)} \\ & + \sum_{j=0}^{\infty} \sum_{i=1}^4 (\pm 1)^j \left(\frac{i(i-1)\nu}{b_p^2} \mu_n^{(i-2)} - \alpha_j^2 \mu_n^{(i)} \right) c_j^{(i)} = 0; \end{aligned} \tag{37a}$$

$(n = 0, 1, 2, \dots)$.

From $\left[\frac{\partial^3 w}{\partial x^3} + (2 - \nu) \frac{\partial^3 w}{\partial x \partial y_1^2} \right]_{x=\mp l} = 0$:

$$\sum_{i=1}^4 \left[\frac{6\delta_{i3}}{l^3} \mp \frac{24\delta_{i4}}{l^3} - (2 - \nu) \tilde{\beta}_n^2 \times \frac{i(\mp 1)^{i+1}}{l} \right] d_n^{(i)} = 0; \tag{37b}$$

$(n = 0, 1, 2, \dots)$

From $\left[\frac{\partial^2 w}{\partial y_1^2} + \nu \frac{\partial^2 w}{\partial x^2} \right]_{y_1=\mp b_p} = 0$:

$$\begin{aligned} & -\sum_{n=0}^{\infty} (\tilde{\beta}_n^2 + \nu \alpha_j^2) (\pm 1)^n C_{nj} + \sum_{i=1}^4 \left[\frac{i(i-1)}{b_p^2} - \nu \alpha_j^2 \right] (\mp 1)^i c_j^{(i)} \\ & + \sum_{n=0}^{\infty} \sum_{i=1}^4 (\pm 1)^n \cdot \left[\frac{i(i-1)\nu}{l^2} \mu_j^{(i-2)} - \tilde{\beta}_n^2 \mu_j^{(i)} \right] d_n^{(i)} = 0; \end{aligned} \tag{37c}$$

$(j = 0, 1, 2, \dots)$

From $\left[\frac{\partial^3 w}{\partial y_1^3} + (2 - \nu) \frac{\partial^3 w}{\partial y_1 \partial x^2} \right]_{y_1=\mp b_p} = 0$:

$$\sum_{i=1}^4 \left[\frac{6\delta_{i3}}{b_p^3} \mp \frac{24\delta_{i4}}{b_p^3} - (2 - \nu) \alpha_j^2 \times \frac{i(\mp 1)^{i+1}}{b_p} \right] c_j^{(i)} = 0; \tag{37d}$$

$(j = 0, 1, 2, \dots)$

Equations (30) and (37) form a linear system of equations for the unknowns C_{nj} , $c_j^{(i)}$, and $d_n^{(i)}$. For practical computation, the infinite series needs to be truncated at a finite value, e.g., at $n = N - 1$ and $j = J - 1$. This gives

$$\mathbf{A} \cdot \mathbf{x} = \mathbf{B}, \tag{38}$$

where \mathbf{x} is a column vector containing $NJ + 4(N + J)$ unknowns, \mathbf{A} is a square matrix of size $NJ + 4(N + J)$, and \mathbf{B} is the known column vector of the same size as \mathbf{x} , depending on the incident wave.

The reflection and transmission coefficients relationship may be used to verify the present procedure. It can be done by applying Green's identity for the velocity potential ϕ and its complex conjugate $\bar{\phi}$ over the entire boundary of the fluid domain or

$$\iint_S \left[\phi \frac{\partial \bar{\phi}}{\partial n} - \bar{\phi} \frac{\partial \phi}{\partial n} \right] dS = 0. \tag{39}$$

The integration over the side walls, the bottom, and the free surface will disappear when the boundary conditions are used. This gives

$$\begin{aligned} \iint_S \left[\phi \frac{\partial \bar{\phi}}{\partial n} - \bar{\phi} \frac{\partial \phi}{\partial n} \right] dS & = \int_{-H}^0 \int_{-b}^b \left[\phi \frac{\partial \bar{\phi}}{\partial x} - \bar{\phi} \frac{\partial \phi}{\partial x} \right]_{x=-\infty}^{x=+\infty} dy dz \\ & + \int \int_{S_p} \left[\phi \frac{\partial \bar{\phi}}{\partial n} - \bar{\phi} \frac{\partial \phi}{\partial n} \right] dS = 0. \end{aligned} \tag{40}$$

For the second integral on the right-hand-side of (40), we use (2)–(4) and convert the surface integral to the line integral, which gives

$$\begin{aligned} & \iint_{S_p} \left[\phi \frac{\partial \bar{\phi}}{\partial n} - \bar{\phi} \frac{\partial \phi}{\partial n} \right] dS \\ & = \frac{L}{\rho} \iint_{S_p} (\bar{w} \nabla^4 w - w \nabla^4 \bar{w}) dS \\ & = \frac{L}{\rho} \times \oint_c \left(\bar{w} \frac{\partial}{\partial n} \nabla^2 w - \frac{\partial \bar{w}}{\partial n} \nabla^2 w - w \frac{\partial}{\partial n} \nabla^2 \bar{w} + \frac{\partial w}{\partial n} \nabla^2 \bar{w} \right) ds. \end{aligned} \tag{41}$$

The line integral is obtained from Gauss's theorem and is along the plate edge. It can be further treated by applying the edge conditions. For example, for the free edge, by using (8), we have

$$\begin{aligned} & \frac{L}{\rho} \times \oint_c \left(\bar{w} \frac{\partial}{\partial n} \nabla^2 w - \frac{\partial \bar{w}}{\partial n} \nabla^2 w - w \frac{\partial}{\partial n} \nabla^2 \bar{w} + \frac{\partial w}{\partial n} \nabla^2 \bar{w} \right) ds, \\ & = \frac{L(1-\nu)}{\rho} \oint_c \frac{\partial}{\partial s} \left(-\bar{w} \left[\frac{\partial^2 w}{\partial s \partial n} - \frac{1}{\mathcal{R}} \frac{\partial w}{\partial s} \right] - \frac{\partial \bar{w}}{\partial n} \frac{\partial w}{\partial s} \right. \\ & \quad \left. + w \left[\frac{\partial^2 \bar{w}}{\partial s \partial n} - \frac{1}{\mathcal{R}} \frac{\partial \bar{w}}{\partial s} \right] + \frac{\partial w}{\partial n} \frac{\partial \bar{w}}{\partial s} \right) ds = 0. \end{aligned} \tag{42}$$

For edge conditions in (7) or (9), (42) can be obtained in a similar way. The left-hand side of (41) is in fact the average work done to the plate by the fluid over one time period or the energy absorbed by the plate, which is zero when there is no structural damping. It is noted that this is valid for a plate of any shape and is not limited to a rectangular one.

Equation (40) then becomes

$$\int_{-H}^0 \int_{-b}^b \left[\phi \frac{\partial \bar{\phi}}{\partial x} - \bar{\phi} \frac{\partial \phi}{\partial x} \right]_{x_0=-\infty}^{x_0=+\infty} dy_0 dz_0 = 0. \tag{43}$$

The expansion of ϕ at infinity can be obtained by taking $x_0 = \pm\infty$ in (16) and keeping only the $n + 1$ progressing wave terms in (11), we have

$$\phi|_{x_0=-\infty} = \phi_I + \sum_{n=0}^{\infty} a_{n0} e^{i\tau_{0n}x_0} \cos \beta_n(y_0 + b) \frac{\cosh k_0(z_0 + H)}{\cosh k_0H} \tag{44}$$

and

$$\phi|_{x_0=+\infty} = \sum_{n=0}^{\infty} c_{n0} e^{-i\tau_{0n}x_0} \cos \beta_n(y_0 + b) \frac{\cosh k_0(z_0 + H)}{\cosh k_0H}, \tag{45}$$

where $n \geq 0$ and

$$\begin{aligned} a_{n0} &= -\frac{k_0^2 \sinh k_0H \cosh k_0H}{\rho \omega b (k_0H + \sinh k_0H \cosh k_0H)} \times \frac{\chi_n^{(-)}}{\tau_{0n}(1 + \delta_{n0})}, \\ c_{n0} &= -\frac{\delta_{n0}g}{i\omega} - \frac{k_0^2 \sinh k_0H \cosh k_0H}{\rho \omega b (k_0H + \sinh k_0H \cosh k_0H)} \times \frac{\chi_n^{(+)}}{\tau_{0n}(1 + \delta_{n0})}, \end{aligned}$$

with

$$\chi_n^{(\pm)} = \iint_{S_p} (L\nabla^4 w - \omega^2 \rho_e h w) \cos \beta_n(y + b) e^{\pm i\tau_{0n}x} dx dy_1, \tag{46}$$

where $n \geq 0$ and $n + 1$ in the above-mentioned equations refer to the number of the traveling wave components. a_{n0} and c_{n0} are, respectively, related to the reflection and transmission coefficients corresponding to each transverse mode of $\cos \beta_n(y + b)$. Substituting (44) and (45) into (43), we obtain the energy identity as

$$\frac{\omega^2}{2g^2 k_0} \sum_{n=0}^{\infty} \tau_{n0} (|a_{n0}|^2 + |c_{n0}|^2) (1 + \delta_{n0}) = 1. \tag{47}$$

This is in fact the same as that in Linton and Evans⁹ for a rigid body in a channel. However, here it is re-derived for an elastic body.

From (47), the squared magnitude of the reflection and transmission coefficients can be defined as

$$|R|^2 = \frac{\omega^2}{2g^2 k_0} \sum_{n=0}^{\infty} (1 + \delta_{n0}) \tau_{n0} |a_{n0}|^2 \tag{48}$$

and

$$|T|^2 = \frac{\omega^2}{2g^2 k_0} \sum_{n=0}^{\infty} (1 + \delta_{n0}) \tau_{n0} |c_{n0}|^2, \tag{49}$$

respectively.

The total vertical force on the horizontal plate can be obtained by the integration of fluid pressure difference p over the surface of the plate S_p . Using (2), the complex vertical force can be given as

$$\begin{aligned} V &= \int_{-l}^l \int_{-b_p}^{b_p} p dx dy_1 \\ &= \int_{-l}^l \int_{-b_p}^{b_p} (L\nabla^4 w - \omega^2 \rho_e h w) dx dy_1 \\ &= 4lb_p \left[\sum_{i=1}^4 \left(-\rho_e h \omega^2 \mu_0^{(i)} + \frac{24L\delta_{i4}}{b_p^4} \right) c_0^{(i)} \right. \\ & \quad \left. + \sum_{i=1}^4 \left(-\rho_e h \omega^2 \mu_0^{(i)} + \frac{24L\delta_{i4}}{l^4} \right) d_0^{(i)} - \rho_e h \omega^2 C_{00} \right]. \end{aligned} \tag{50}$$

Similarly, we can also obtain the moment about the transverse centerline of the plate, or $x = 0$, as

$$\begin{aligned} M_y &= - \int_{-l}^l \int_{-b_p}^{b_p} p x dx dy_1 \\ &= - \int_{-l}^l \int_{-b_p}^{b_p} (L\nabla^4 w - \omega^2 \rho_e h w) x dx dy_1 \\ &= 2l^2 b_p \rho_e h \omega^2 \sum_{j=1}^{\infty} \left[C_{0j} + \sum_{i=1}^4 d_0^{(i)} \mu_j^{(i)} + \sum_{i=1}^4 c_j^{(i)} \mu_0^{(i)} \right] \mu_j^{(1)} \\ & \quad - 2l^2 b_p L \sum_{j=1}^{\infty} \left[\alpha_j^4 C_{0j} + \left(\frac{\alpha_j^4}{3} - \frac{4\alpha_j^2}{b_p^2} \right) c_j^{(2)} + \left(\frac{24}{b_p^4} + \frac{\alpha_j^4}{5} - \frac{8\alpha_j^2}{b_p^2} \right) c_j^{(4)} \right] \mu_j^{(1)}, \end{aligned} \tag{51}$$

and the moment about the longitudinal centerline of the plate, or $y_1 = 0$, as

$$\begin{aligned} M_x &= \int_{-l}^l \int_{-b_p}^{b_p} p y_1 dx dy_1 \\ &= \int_{-l}^l \int_{-b_p}^{b_p} (L\nabla^4 w - \omega^2 \rho_e h w) y_1 dx dy_1 \\ &= 2lb_p^2 L \sum_{n=1}^{\infty} \left[\tilde{\beta}_n^4 C_{n0} + \left(\frac{\tilde{\beta}_n^4}{3} - \frac{4\tilde{\beta}_n^2}{l^2} \right) d_n^{(2)} + \left(\frac{\tilde{\beta}_n^4}{5} - \frac{8\tilde{\beta}_n^2}{l^2} + \frac{24}{l^4} \right) d_n^{(4)} \right] \mu_n^{(1)} \\ & \quad - 2lb_p^2 \rho_e h \omega^2 \sum_{n=1}^{\infty} \left(C_{n0} + \sum_{i=1}^4 \mu_0^{(i)} a_n^{(i)} + \sum_{i=1}^4 \mu_n^{(i)} c_0^{(i)} \right) \mu_n^{(1)}. \end{aligned} \tag{52}$$

The elevation of the diffracted waves can be calculated as

$$\eta_D(x_0, y_0) = -\frac{i\omega}{g} \phi_D|_{z_0=0} = -\sum_{n=0}^{\infty} \sum_{j=0}^{\infty} \frac{\mathcal{M}_{nj}}{2\rho gb} \sum_{n'=0}^{\infty} \frac{\cos \beta_{n'}(y_0 + b) I_1^{(n,n')}}{(1 + \delta_{n'0})} \sum_{m=0}^{\infty} \frac{k_m \cosh k_m H \sinh k_m H}{(2k_m H + \sinh 2k_m H)} \mathfrak{D}_{m,n',j}, \tag{53}$$

where

$$\mathfrak{D}_{m,n',j} = \begin{cases} \frac{e^{i\tau_{mn'}(x_0-l)} [-e^{2i\tau_{mn'}l} + (-1)^j]}{\tau_{mn'}^2 - \alpha_j^2}, & x_0 < -l \\ \frac{2 \cos \alpha_j(l + x_0) - e^{-i\tau_{mn'}l} [(-1)^j e^{i\tau_{mn'}x_0} + e^{-i\tau_{mn'}x_0}]}{\alpha_j^2 - \tau_{mn'}^2}, & -l < x_0 < l \\ \frac{e^{-i\tau_{mn'}(x_0+l)} [-e^{2i\tau_{mn'}l}(-1)^j + 1]}{\tau_{mn'}^2 - \alpha_j^2}, & x_0 > l \end{cases} \tag{54}$$

and

$$\begin{aligned} \mathcal{M}_{nj} = C_{nj} & \left[L(\alpha_j^2 + \tilde{\beta}_n^2)^2 - \omega^2 \rho_e h \right] + \sum_{i=1}^4 \left[L \left(\alpha_j^4 \mu_n^{(i)} - \frac{2i(i-1)}{b_p^2} \alpha_j^2 \mu_n^{(i-2)} + \frac{24\delta_{i4} \mu_n^{(0)}}{b_p^4} \right) - \omega^2 \rho_e h \mu_n^{(i)} \right] c_j^{(i)} \\ & + \sum_{i=1}^4 \left[L \left(\tilde{\beta}_n^4 \mu_j^{(i)} - \frac{2i(i-1)}{l^2} \tilde{\beta}_n^2 \mu_j^{(i-2)} + \frac{24\delta_{i4} \mu_j^{(0)}}{l^4} \right) - \omega^2 \rho_e h \mu_j^{(i)} \right] d_n^{(i)}. \end{aligned} \tag{55}$$

III. RESULTS AND ANALYSIS

Dimensionless variables are adopted for calculation and analysis based on the following three characteristic variables and their combinations: the half-width of the plate b_p , the acceleration due to gravity g , and the water density ρ .

A. Centrally located floating plates

We begin by considering a plate situated at the center of the channel, or $y_c = 0$ and the four edges of the plate are assumed as free, or F-F-F-F. The graphs of $|V|$ and $|M_y|$ against wave frequencies are shown in Figs. 2(a) and 2(b), respectively, with $M_x = 0$ due to symmetry. Specifically, when $b = b_p$, a series expansion method is also employed to solve the problem,²⁹ and the results are displayed in Fig. 2 for verification. The figure shows that the boundary integral scheme and the alternative method produce virtually identical results, demonstrating the validity of both schemes. In addition, results of other values of b , namely, $b = 2.0$ and 3.0 , obtained from the boundary integral scheme, are also provided in Fig. 2. In addition, to evaluate the convergence of the truncated infinite series in practical computations, we utilize three different sets of truncation numbers (N, J), specifically (50, 20), (50, 30), and (60, 20), for 24 discrete wave frequencies in the case of $b = 3$. The obtained results hardly show any visible difference, particularly in regions where the curve does not exhibit abrupt variations, as depicted in Fig. 2(a). We may observe that the curves of $|V|$ and $|M_y|$ are very close to each other for different b at relatively small wave frequencies. This is because when the frequency is low, the wave force is predominantly due to incident waves. The incident wave is two dimensional, and its force is, therefore, not affected by b . As the wave frequency increases, these curves corresponding to different b start to diverge from one another, illustrating that the wave diffraction

becomes more important and that the effect of the side walls becomes more evident. Transversely, a larger value of b indicates a wider free surface area between the plate edge and the side wall. It is worth noting that within the same frequency range, the curves tend to be more oscillatory with the increase in b . From (10), it can be seen that when $\tau_{0n} = 0$, or $k_0 = \beta_n = n\pi/2b$, the Green function is infinite, which in fact corresponds to the natural frequencies of the channel. When b is larger, the two successive natural frequencies at n and $n + 1$ are closer to each other, leading to more oscillations in the curves. For the case of $b = 3$, as it is a symmetric case, the frequencies corresponding to $k_0 = n\pi/6$ (even $n = 2, 4, 6, \dots$) are at $\omega_n = \sqrt{(gn\pi/6) \tanh(n\pi H/6)}$, where rapid variation may occur, as can be seen from the figure. We can find that the variations at some ω_n are less evident than those at other ones, for instance, at $\omega_8, \omega_{14}, \omega_{20}, \omega_{22}, \omega_{28}$, etc. In fact, we may refer to the work of Wu,¹³ which investigated wave radiation and diffraction by a sphere in a channel. The exciting force displayed in Fig. 3(b) shows mild variation at ω_n , while variations of radiation force or the added mass and damping coefficients, respectively, in Figs. 1(c) and 2(c) are much more noticeable. Here, the force includes both the excitation force and the radiation force. It is worth noting that the radiation force becomes significant only when motion is significant. In this context, the variation of V may be evident at ω_n , only when the deflection of the plate w is not small. Furthermore, it should be noted that there are other causes for oscillation, which are discussed later. Moreover, the $|M_y|$ curve for $b = 3$ in Fig. 2(b) demonstrates a more oscillatory behavior compared with that for $b = 2$, similar to the $|V|$ curves. However, these oscillations are accompanied by a significantly reduced amplitude.

We then consider the case of $b = 3.0$ with different l , specifically $l = 1.5$ and 2.0 . We show the $|V|$ and $|M_y|$ curves in Figs. 3(a) and 3(b), respectively. It is expected that the oscillation at $k_0 = \beta_n = n\pi/2b$ mentioned above occurs at the same place for different l .

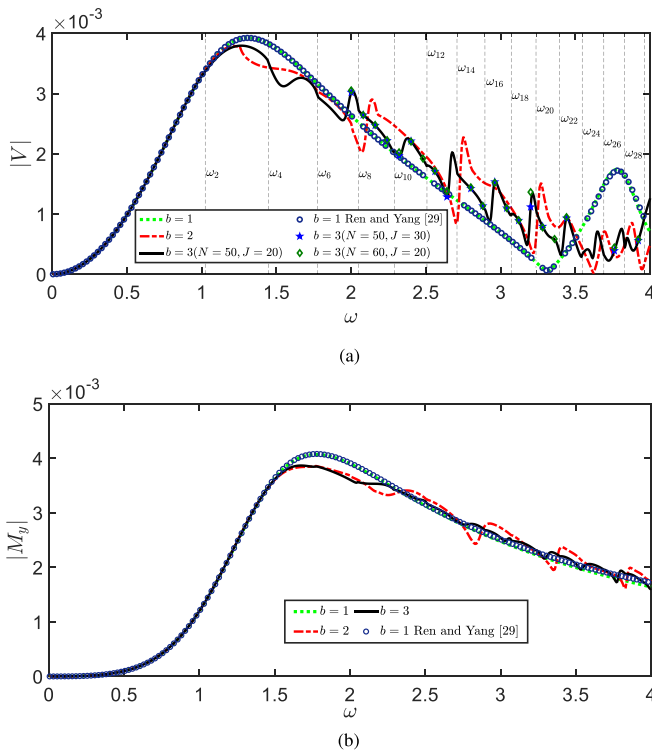


FIG. 2. Modulus of (a) the total vertical force and (b) the moment about $x = 0$ on a centrally located plate with free edge conditions (F-F-F-F). In (a), the vertical dashed lines indicate ω_n ($n = 2, 4, 6, \dots$) for $b = 3$. Here, $l = 1$, $b_p = 1$, $H = 4$, $\rho_0 h = 1 \times 10^{-3}$, $L = 0.1$.

In fact, the oscillation of the curves in Fig. 3 is due to a combined effect of both b and l . Based on the approximate 2D analysis,^{30,31} there would be another oscillation related to l in the form of $e^{2i\kappa_0 l}$, where κ_0 represents the real solution of the dispersion relationship corresponding to the elastic plate surface. The period of the oscillation will be around $\kappa_0 l = \pi$, which means that if one of the positions is identified, then others can be located. To better illustrate such oscillations, we fix the wave frequency ω corresponding to $\kappa_0 = \pi/2$ and change l and plot the curves of reflection coefficients and wave loads against l in Fig. 4. As can be seen, one of the oscillation components has a period of 2. Furthermore, according to the 2D results, there are certain discrete frequencies at which the reflection coefficients can reach zero, as illustrated by Meylan and Squire.³⁰ However, it is worth noting that this may not be always valid in the three-dimensional scenario when $b > b_p$, as can be observed in Fig. 4(b).

We next investigate how the flexural rigidity affects the force curves by keeping all other parameters fixed but varying L . Figure 5 shows the curves of $|V|$ and $|M_y|$ as L increases from 0.0001 to 20. Notably, by comparing the results of $L = 10$ and $L = 20$, it is evident that a further increase in L will not significantly change the curve anymore. It is expected that when L approaches infinity, the results will tend to those corresponding to a rigid plate. In fact, at $L = +\infty$, only linear terms in w need to be retained and the dynamic equation of the plate can be converted to those associated with the heave, pitch, and roll motions of a rigid body.

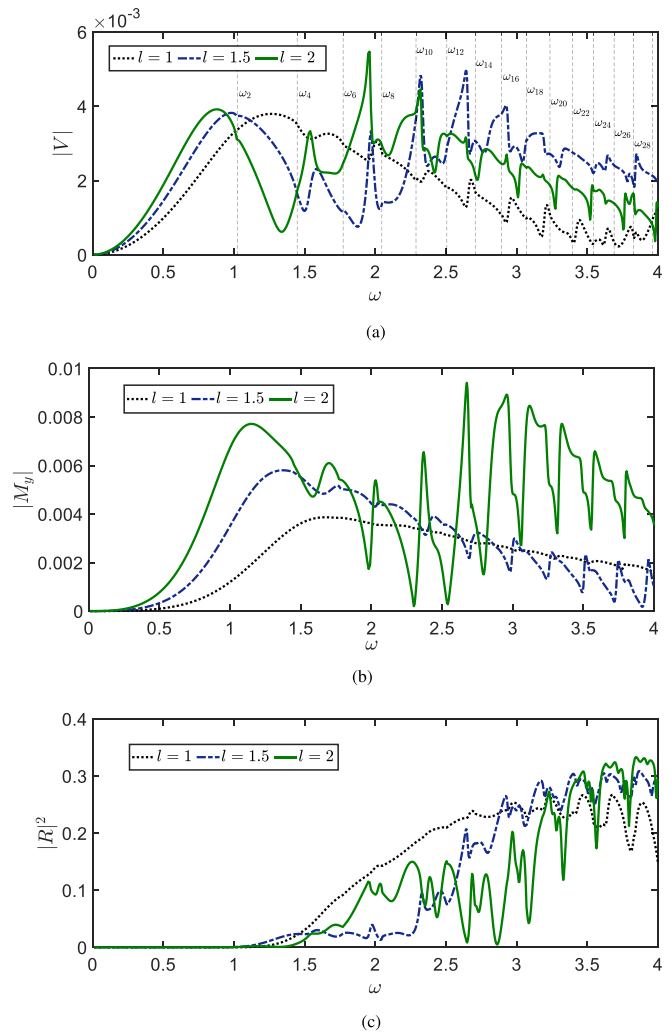


FIG. 3. Modulus of (a) vertical force, (b) moment about $x = 0$, and (c) squared magnitude of the reflection coefficients on a central-located plate with free edge conditions (F-F-F-F), for $l = 1.5$ and 2.0. Here, $b_p = 1$, $b = 3$, $H = 4$, $\rho_0 h = 1 \times 10^{-3}$, $L = 0.1$.

B. Effects of different edge conditions

The solution procedure presented in Sec. II can be readily adapted to other types of edge conditions. This can be accomplished, for instance, by modifying the linear equations in Eq. (37) to accommodate the relevant edge conditions. For clamped edges located at $y_1 = \pm b_p$, the zero-deflection and zero-slope conditions yield

$$\sum_{n=0}^{\infty} (\pm 1)^n C_{nj} + \sum_{n=0}^{\infty} \sum_{i=1}^4 (\pm 1)^n \mu_j^{(i)} d_n^{(i)} + \sum_{i=1}^4 (\mp 1)^i c_j^{(i)} = 0$$

from $w|_{y_1=\pm b_p} = 0$,

(56a)

$$\sum_{i=1}^4 i \times (\mp 1)^{i-1} \times c_j^{(i)} = 0 \quad \text{from } w_{y_1}|_{y_1=\pm b_p} = 0 \quad (j = 0, 1, 2, \dots)$$
(56b)

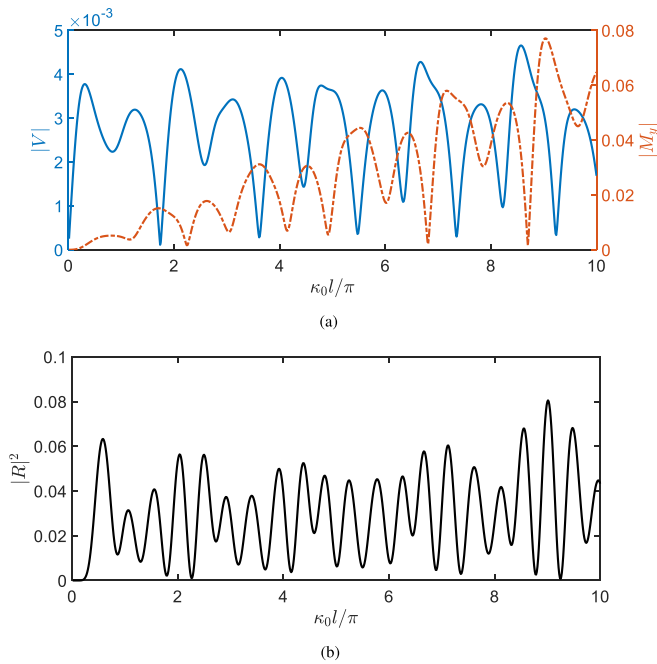


FIG. 4. Modulus of (a) vertical force and moment about $x = 0$ and (b) squared magnitude of the reflection coefficients on a central-located plate with free edge conditions (F-F-F-F) against l at $\kappa_0 l = \pi/2$. Here, $b_p = 1, b = 3, H = 4, \rho_e h = 1 \times 10^{-3}, L = 0.1$.

while for simply supported edges at $y_1 = \pm b_p$, (56a) and (37c) can be used to impose the zero-deflection and zero-bending moment conditions, respectively. Moreover, the elastically supported edge conditions can also be considered by using (37d) for zero-Kirchhoff shear force condition, and

$$-L \left[\frac{\partial^2 w}{\partial y_1^2} + \nu \frac{\partial^2 w}{\partial x^2} \right]_{y_1 = \mp b_p} = K \left[\frac{\partial w}{\partial y_1} \right]_{y_1 = \mp b_p} \quad (57a)$$

or

$$\begin{aligned} & -L \left\{ - \sum_{n=0}^{\infty} (\tilde{\beta}_n^2 + \nu \alpha_j^2) (\pm 1)^n C_{nj} + \sum_{i=1}^4 \left[\frac{i(i-1)}{b_p^2} - \nu \alpha_j^2 \right] (\mp 1)^i c_j^{(i)} \right. \\ & \left. + \sum_{n=0}^{\infty} \sum_{i=1}^4 (\pm 1)^n \cdot \left[\frac{i(i-1)\nu}{l^2} \mu_j^{(i-2)} - \tilde{\beta}_n^2 \mu_j^{(i)} \right] d_n^{(i)} \right\} \\ & = K \sum_{i=1}^4 i \times (\mp 1)^{i-1} \times c_j^{(i)} \quad (j = 0, 1, 2, \dots), \end{aligned} \quad (57b)$$

showing that shear force linked to rotation at the edge could be countered by spiral springs with distributed stiffness K .

To further investigate the effects of various edge conditions, we maintain the free edge conditions at the edges of $x = \pm l$, while introducing various edge types at $y_1 = \pm b_p$, specifically with the following combinations: free-free (F-F), clamped-clamped (C-C), clamped-free (C-F), clamped-simply supported (C-SS), simply supported-simply supported (SS-SS), and simply supported-free (SS-F). The results of

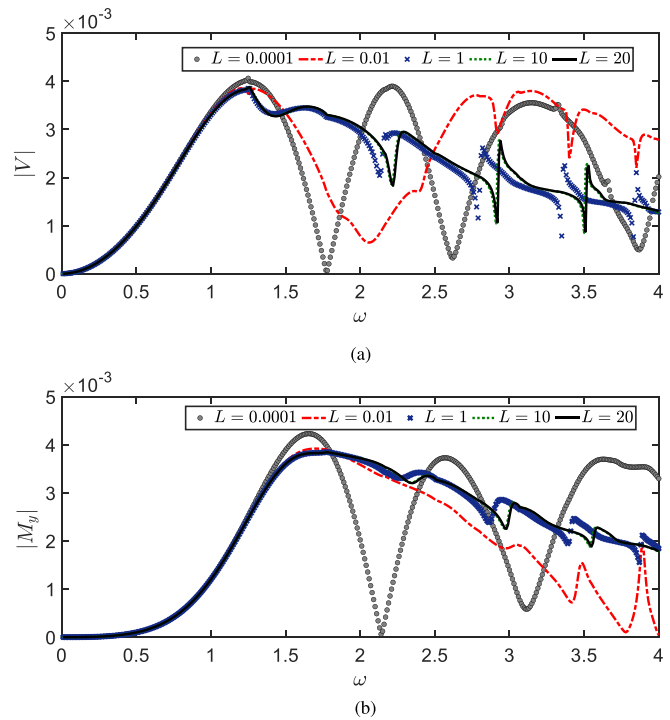


FIG. 5. Modulus of (a) vertical force and (b) moment about $x = 0$ on a central-located plate with free edge conditions (F-F-F-F) of different L . Here, $l = 1, b_p = 1, b = 2, H = 4, \rho_e h = 1 \times 10^{-3}$.

the squared magnitude of reflection and transmission coefficients for $b_p = b$ are presented in Fig. 6. To provide some comparison, the results for the corresponding 2D case are provided. For a rigid plate with $b_p = b$ in the channel, the result will be the same as the 2D one. For an elastic plate, the problem is strictly 3D, because of the edge conditions. In fact, the figure shows that the patterns of curves are very different from that of the 2D one. One exception is the F-F edge case, whose result is much closer to the 2D one, especially at lower frequencies.

Figure 7 displays the plots of $|V|$ and $|M_y|$ as ω varies, for three edge types, namely, C-C, SS-SS, and C-SS, at $y_1 = \pm b_p$. From the figure, it is observed that the forces and moments associated with these three cases exhibit considerably larger magnitudes compared to those of the F-F case (the corresponding values are marked in Fig. 7, scaled up by a factor of 1000). This is because these edges effectively led to a stiffer structural response, while the free edges in the F-F case allow for greater flexibility of motion. Take the C-C case for instance, when both edges of the plate parallel to the channel walls are clamped, the deformations and slopes at these edges are constrained to zero. This restricts its ability to bend and deform under the applied loads, and as a result, the forces and moments experienced by the plate tend to be notably higher. In contrast, in the F-F case where both edges are free to move, the plate can move and deform more freely in response to the applied loads. This results in much smaller forces and moments compared to the C-C scenario.

We extend our investigation to cases with $b > b_p$ through a case of $b = 2.0$. The edges at $x = \pm l$ remain to be free, while the edges at

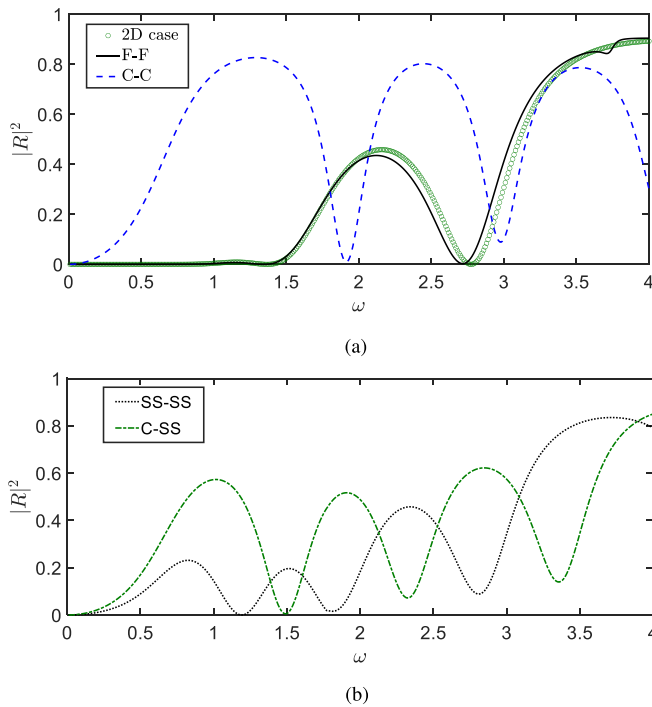


FIG. 6. $|R|^2$ against ω under different edge types at $y_1 = \pm b_p$: (a) **F-F** and **C-C**; (b) **SS-SS** and **C-SS**. Here, $l = 2$, $b_p = b = 1$, $H = 4$, $\rho_e h = 1 \times 10^{-3}$, $L = 0.1$.

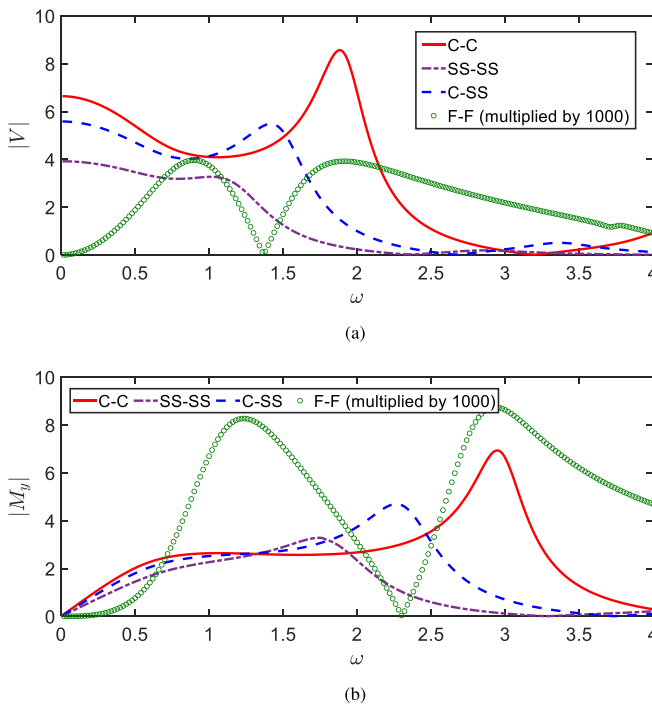


FIG. 7. The curves of (a) $|V|$ and (b) $|M_y|$ with varying ω under different edge types along the channel banks. Here, $l = 2$, $b_p = b = 1$, $H = 4$, $\rho_e h = 1 \times 10^{-3}$, $L = 0.1$.

$y_1 = \pm b_p$ are clamped. The curves of $|R|^2$ and $|T|^2$, $|V|$ and $|M_y|$ are displayed in Figs. 8(a) and 8(b), respectively. The figures show that the results in this case are much more oscillatory than those at $b_p = b$. It can be observed that at the peaks of $|T|^2$, the vertical force $|V|$ is also at a peak.

C. Off-center floating plates

In this section, we investigate cases involving an off-center floating plate, with $|y_c| > 0$. We analyze how the fluid loads acting on the plate change as $|y_c|$ increases, at several discrete wave frequencies. Specifically, we set the parameters as $l = 2$, $b = 2$, $H = 4$, with ω ranging from 0.5 to 2.0 with an interval of 0.5. The results for two edge cases, namely, **F-F** and **C-C**, are presented in Fig. 9.

For **F-F** cases, as can be observed in Figs. 9(a), 9(c), and 9(e), the curves of $|V|$, $|M_y|$, and $|M_x|$ are very close to each other for different y_c at relatively small wave frequencies. This indicates that the force is predominantly independent of the horizontal position of the plate when the incident wave has a relatively longer wavelength, implying that the wave diffraction is negligible and the force is mainly due to the incident wave. However, as the wave frequency increases, these curves corresponding to different offset values start to diverge from one another, illustrating that the wave diffraction becomes more important and that the effect of the side walls becomes more evident. In contrast, in **C-C** cases, notable distinctions become apparent when compared to **F-F** cases. As shown in Figs. 9(b), 9(d), and 9(f), we observe substantial curve variations with y_c , even at relatively small wave frequencies such

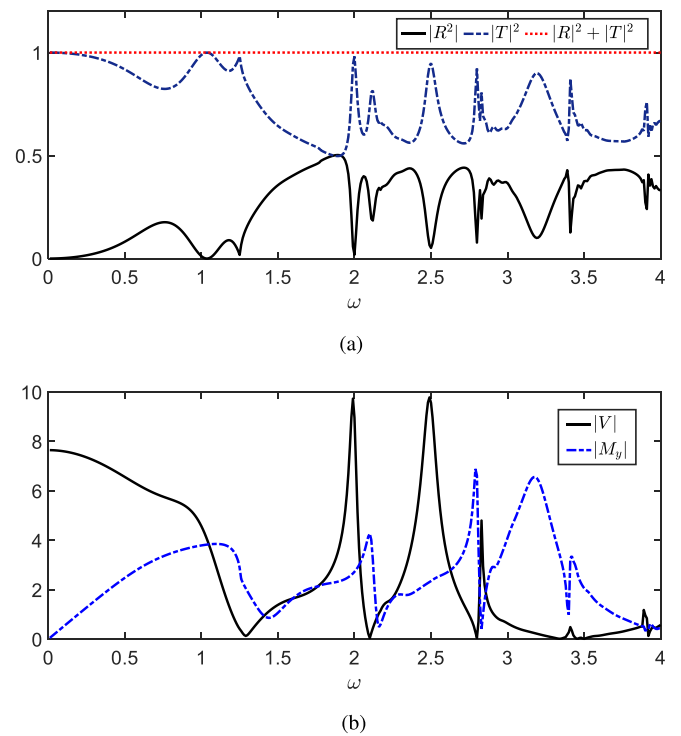


FIG. 8. Variations of (a) $|R|^2$ and $|T|^2$ and (b) $|V|$ and $|M_y|$ against ω under clamped edge types at $y_1 = \pm b_p$. Here, $l = 2$, $b = 2$, $H = 4$, $\rho_e h = 1 \times 10^{-3}$, $L = 0.1$.

21 August 2024 10:19:07

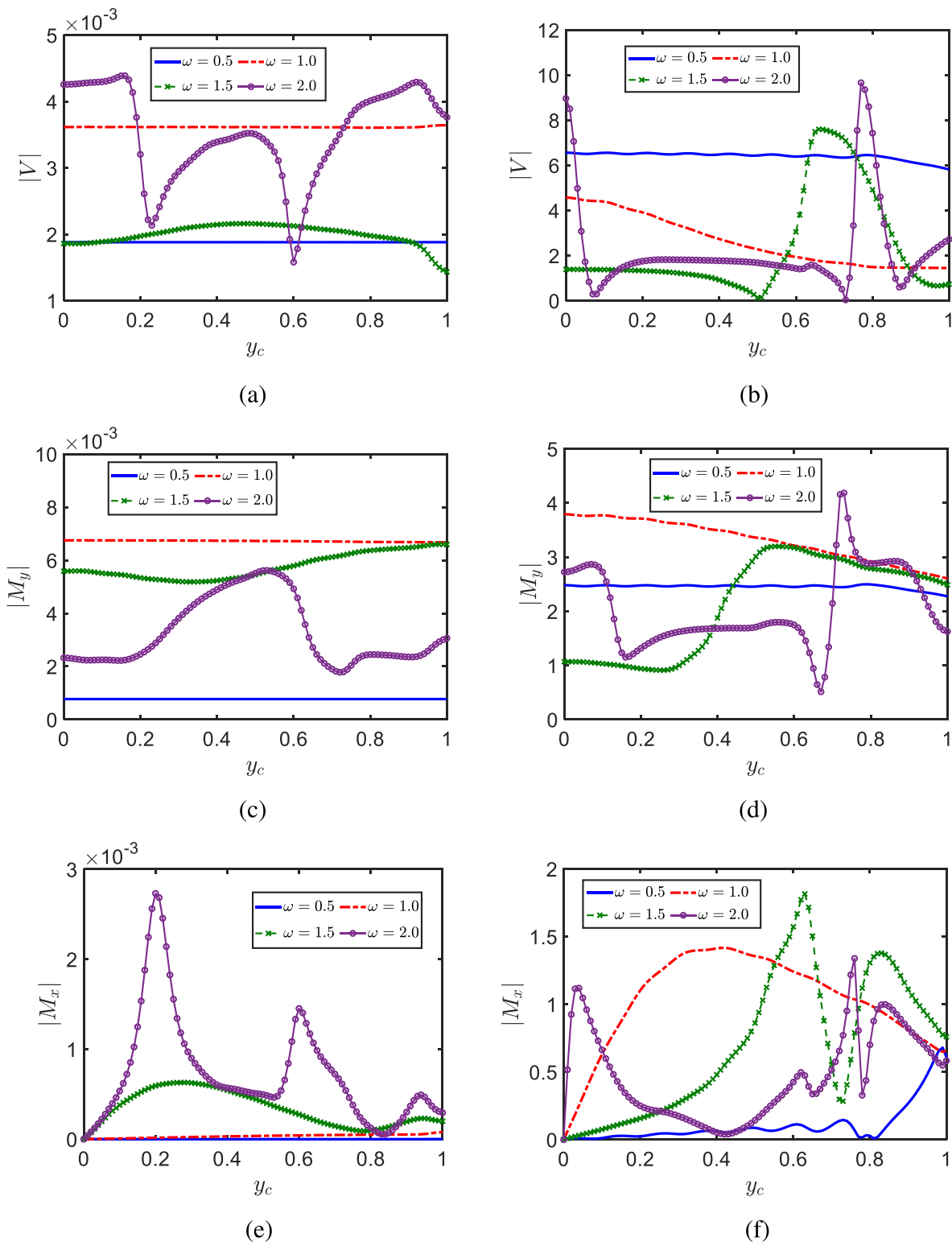


FIG. 9. Modulus of fluid loads under different ω at varying $|y_c|$: (a) $|V|$ for F-F; (b) $|V|$ for C-C; (c) $|M_y|$ for F-F; (d) $|M_y|$ for C-C; (e) $|M_x|$ for F-F; (f) $|M_x|$ for C-C. Here, $l = 2$, $b = 2$, $H = 4$, $\rho_\theta h = 1 \times 10^{-3}$, $L = 0.1$.

as $\omega = 0.5$ and 1.0 . This variation arises due to the increased prominence of wave diffraction induced by the plate with clamped edges along its longitudinal sides.

D. Wave profiles and plate deformation

Following the previous analysis, this section delves into the deformations of the plate and the diffracted wave profile, as determined from Eqs. (25) and (53). We have noted from the finding in Fig. 8 that for C-C edges at $y = \pm b_p$, the peak of $|V|$ aligns with the peak of $|T|^2$ at specific discrete frequencies. The modulus of the plate deformation and the surrounding diffracted free surface profile are, respectively, displayed in Figs. 10(a) and 10(b) at $\omega = 2.0$ and $\omega = 2.5$. For comparison, the graphs for F-F edges are also provided in Figs. 10(c) and 10(d). The color bar limits for these four graphs have been set to a consistent range of 0–4 for convenience in comparing these wave profiles.

From Fig. 10, we can observe from these graphs that in both C-C and F-F cases, the increase in the wave frequency results in more complex wave profiles, indicating an increased influence of the diffraction effects. At the same wave frequency, the diffraction wave profiles in

C-C cases are generally larger than those in F-F cases. Specifically, in the C-C case, we observe that the wave profiles on the upstream side ($x < -l$) remain relatively low at both the examined frequencies, consistent with the locations of the troughs in $|R|^2$ at these discrete frequencies. At $\omega = 2.0$, significant wave elevations persist in the region between the two longitudinal edges of the plate and the channel walls. In contrast, for $\omega = 2.5$, large wave elevations are observed predominantly on the downstream side ($x > l$).

IV. CONCLUSIONS

The interaction of a surface wave and a finite elastic rectangular plate floating at any position in a channel has been investigated. An analytical solution scheme using the Green function method has been developed, which is based on the linear velocity potential flow theory for the fluid flow and the Kirchhoff–Love plate theory for the plate. This approach can be used efficiently for a plate of any edge constraints, and both centrally located and off-center positions. We can draw the following key conclusions through extensive investigations into the response of plate and the associated wave phenomena:

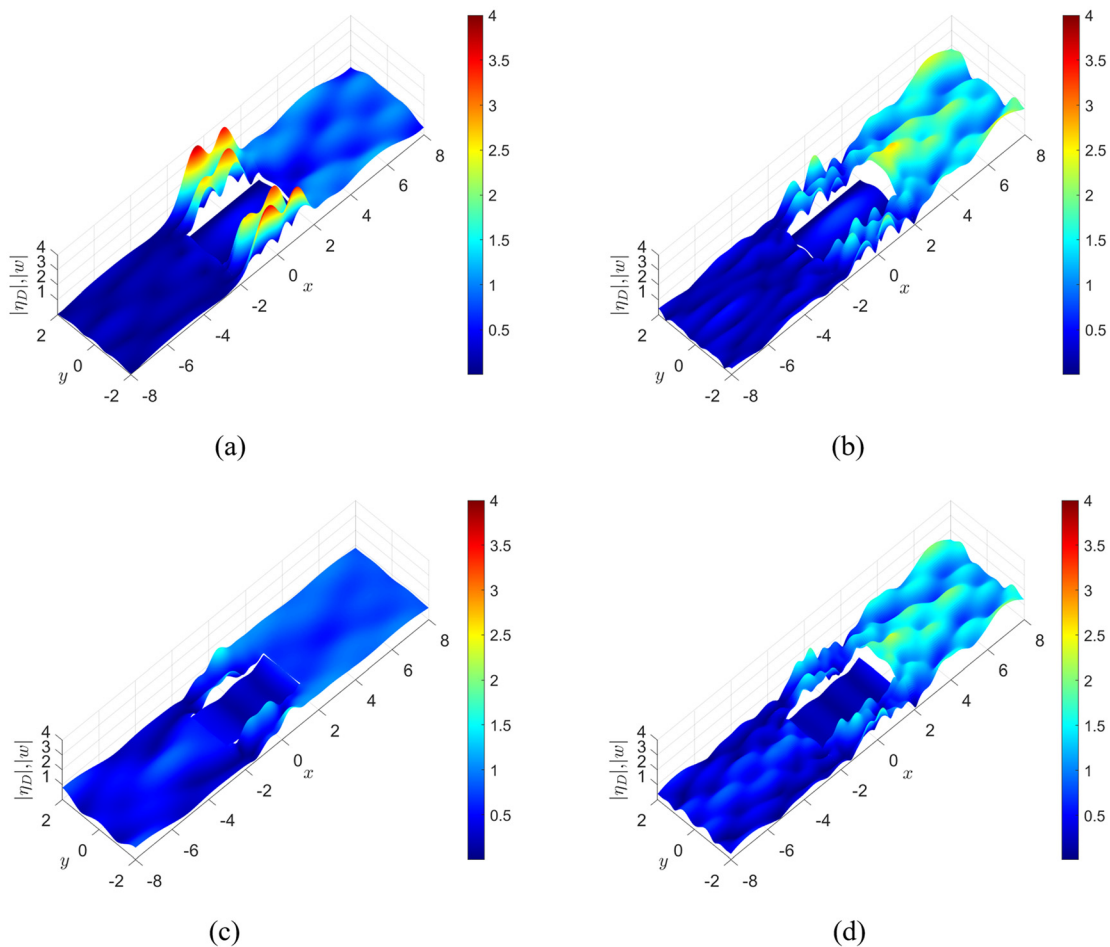


FIG. 10. Modulus of the plate deflection and the diffracted wave profile under C-C and F-F edges at $y = \pm b_p$: (a) $\omega = 2.0$ under C-C edge; (b) $\omega = 2.5$ under C-C edge; (c) $\omega = 2.0$ under F-F edge; and (d) $\omega = 2.5$ under F-F edge. Here, $l = 2$, $b_p = 1$, $b = 2$, $y_c = 0$, $H = 4$, $\rho_p h = 1 \times 10^{-3}$, $L = 0.1$.

21 August 2024 10:19:07

- (1) The highly oscillatory feature of force curves is due to a variety of factors, including the natural frequency effect of the tank related to its width and successive reflections from the edges of the plate related to the length. At some natural frequencies, the oscillation amplitudes are smaller than those at other natural frequencies, due to a smaller motion of the plate or, therefore, smaller radiation force.
- (2) Different edge conditions reveal significant variations in the forces on the plate, as they include the radiation force, which is very much influenced by the structural response.
- (3) The variation of the force with the transverse position of the plate is more notable when its two longitudinal edges are clamped (C-C), compared with the force of F-F edges. This is partly because in the case of F-F edges, the plate can more freely follow the wave, resulting a less disturbance to the wave, while the force due to the incident wave is independent of the transverse position of the plate.

This research can also provide valuable insights into the practical implementation of floating photovoltaic systems³² and the development of flexible wave energy conservation devices³³ that can be effectively utilized in both natural rivers and confined water bodies.

ACKNOWLEDGMENTS

Kang Ren would like to acknowledge the NEST funding received from the Lloyd's Register Foundation (Nos. N\100012 and N21\100005) and the funding from the Royal Society (No. IEC\NSFC\223358) for developing marine renewable energy.

AUTHOR DECLARATIONS

Conflict of Interest

The authors have no conflicts to disclose.

Author Contributions

Kang Ren: Conceptualization (lead); Funding acquisition (lead); Investigation (lead); Methodology (lead); Writing – original draft (lead); Writing – review & editing (lead). **Guoxiong Wu:** Conceptualization (lead); Investigation (lead); Methodology (lead); Writing – original draft (equal); Writing – review & editing (lead). **Yifeng Yang:** Investigation (supporting); Writing – review & editing (supporting).

DATA AVAILABILITY

The data that support the findings of this study are available within the article.

REFERENCES

- ¹R. Eatock Taylor and S. M. Hung, “Mean drift forces on an articulated column oscillating in a wave tank,” *Appl. Ocean Res.* **7**(2), 66–78 (1985).
- ²R. W. Yeung and S. H. Sphaier, “Wave-interference effects on a truncated cylinder in a channel,” *J. Eng. Math.* **23**(2), 95–117 (1989).
- ³C. M. Linton and D. V. Evans, “The radiation and scattering of surface waves by a vertical circular cylinder in a channel,” *Philos. Trans. R Soc. London A* **338**(1650), 325–357 (1992).
- ⁴P. McIver and G. S. Bennett, “Scattering of water waves by axisymmetric bodies in a channel,” *J. Eng. Math.* **27**(1), 1–29 (1993).
- ⁵C. M. Linton and P. McIver, “The scattering of water waves by an array of circular cylinders in a channel,” *J. Eng. Math.* **30**(6), 661–682 (1996).
- ⁶F. Ursell, “Trapping modes in the theory of surface waves,” *Math. Proc. Camb. Philos. Soc.* **47**(2), 347–358 (1951).
- ⁷F. Ursell, “Mathematical aspects of trapping modes in the theory of surface waves,” *J. Fluid Mech.* **183**, 421–437 (1987).
- ⁸P. McIver, “Trapping of surface water waves by fixed bodies in a channel,” *Q. J. Mech. Appl. Math.* **44**(2), 193–208 (1991).
- ⁹C. M. Linton and D. V. Evans, “Hydrodynamic characteristics of bodies in channels,” *J. Fluid Mech.* **252**, 647–666 (1993).
- ¹⁰D. V. Evans and R. Porter, “Trapped modes about multiple cylinders in a channel,” *J. Fluid Mech.* **339**, 331–356 (1997).
- ¹¹S. A. Nazarov and J. H. Videman, “Trapping of water waves by freely floating structures in a channel,” *Proc. R. Soc. A* **467**(2136), 3613–3632 (2011).
- ¹²G. X. Wu, “Wavemaking resistance on a submerged sphere in a channel,” *J. Ship Res.* **42**(01), 1–8 (1998).
- ¹³G. X. Wu, “Wave radiation and diffraction by a submerged sphere in a channel,” *Q. J. Mech. Appl. Math.* **51**(4), 647–666 (1998).
- ¹⁴F. Ursell, “On the wave motion near a submerged sphere between parallel walls: I. Multipole potentials,” *Q. J. Mech. Appl. Math.* **52**, 585–604 (1999).
- ¹⁵F. Ursell, “On the wave motion near a submerged sphere between parallel walls: II. Notes on convergence,” *Q. J. Mech. Appl. Math.* **52**, 605–621 (1999).
- ¹⁶F. Ursell, “The waves due to a submerged sphere moving in a canal,” *Q. J. Mech. Appl. Math.* **57**(3), 335–346 (2004).
- ¹⁷E. Renzi and F. Dias, “Resonant behaviour of an oscillating wave energy converter in a channel,” *J. Fluid Mech.* **701**, 482–510 (2012).
- ¹⁸A. A. Korobkin, T. I. Khabakhpasheva, and A. A. Papin, “Waves propagating along a channel with ice cover,” *Eur. J. Mech.-B/Fluids* **47**, 166–175 (2014).
- ¹⁹K. Ren, G. X. Wu, and Z. F. Li, “Hydroelastic waves propagating in an ice-covered channel,” *J. Fluid Mech.* **886**, A18 (2020).
- ²⁰Y. F. Yang, G. X. Wu, and K. Ren, “Three-dimensional interaction between uniform current and a submerged horizontal cylinder in an ice-covered channel,” *J. Fluid Mech.* **928**, A4 (2021).
- ²¹Y. F. Yang, G. X. Wu, and K. Ren, “Hydroelastic wave diffraction by a vertical circular cylinder standing in a channel with an ice cover,” *J. Fluid Mech.* **941**, A13 (2022).
- ²²A. Dolatshah, F. Nelli, L. G. Bennetts, A. Alberello, M. H. Meylan, J. P. Monty, and A. Toffoli, “Hydroelastic interactions between water waves and floating freshwater ice,” *Phys. Fluids* **30**(9), 091702 (2018).
- ²³Q. Wang, H. Liu, Y. Fang, and F. Dias, “Experimental study on free-surface deformation and forces on a finite submerged plate induced by a solitary wave,” *Phys. Fluids* **32**(8), 086601 (2020).
- ²⁴R. Porter, “The coupling between ocean waves and rectangular ice sheets,” *J. Fluids Struct.* **84**, 171–181 (2019).
- ²⁵K. Ren, G. X. Wu, and Y. F. Yang, “Coupled free vibrations of liquid in a three-dimensional rectangular container with an elastic cover,” *Phys. Fluids* **34**(6), 067109 (2022).
- ²⁶P. A. Martin and L. Farina, “Radiation of water waves by a heaving submerged horizontal disc,” *J. Fluid Mech.* **337**, 365–379 (1997).
- ²⁷S. Timoshenko and S. Woinowsky-Krieger, *Theory of Plates and Shells* (McGraw-Hill, New York, 1959).
- ²⁸C. M. Linton, “On the free-surface Green’s function for channel problems,” *Appl. Ocean Res.* **15**(5), 263–267 (1993).
- ²⁹K. Ren and Y. F. Yang, (2023). “Water wave interaction with a floating finite rectangular plate in a channel,” *The 38th International Workshop on Water Waves and Floating Bodies (IWWWFB)*, Ann Arbor, MI, USA.
- ³⁰M. Meylan and V. A. Squire, “Finite-floe wave reflection and transmission coefficients from a semi-infinite model,” *J. Geophys. Res.* **98**(C7), 12537–12542, <https://doi.org/10.1029/93JC00940> (1993).
- ³¹Y. Y. Shi, Z. F. Li, and G. X. Wu, “Interaction of wave with multiple wide polynyas,” *Phys. Fluids* **31**, 067111 (2019).
- ³²R. J. Schmitt, N. Kittner, G. M. Kondolf, and D. M. Kammen, “Deploy diverse renewables to save tropical rivers,” *Nature* **569**(7756), 330–332 (2019).
- ³³E. Renzi, “Hydroelectromechanical modelling of a piezoelectric wave energy converter,” *Proc. R. Soc. A* **472**(2195), 20160715 (2016).